Supplementary Information for

Non-hazardous and Fully Recyclable Ionic Thermoelectrics for Sustainable Human-Machine Interfaces

Jingyi Yang [1,#], Zifeng Wang [1,#], Zijie Yang [1], Mengmeng Liu [1], David Kwok Hung Lee [2], Ka Bian [2], Jianyong Ouyang [1], Benjamin C. K. Tee [1,2,3,4*]

[1] Department of Materials Science and Engineering, National University of Singapore, Singapore

[2] Institute for Health Innovation and Technology (iHealthtech), National University of Singapore, Singapore

[3] Department of Electrical and Computer Engineering, National University of Singapore, Singapore

[4] The N.1 Institute for Health, National University of Singapore, Singapore

[#] These authors contributed equally.

[*] Correspondence to: benjamin.tee@nus.edu.sg

This supplementary information file includes:

- Supplementary Notes 1 to 4
- Supplementary Figures 1 to 30
- Supplementary Tables 1 to 7
- Supplementary References 1 to 3

Supplementary Notes

Supplementary Note 1: Degradation mechanisms of the ReCLEAR hydrogel.

The degradation mechanism of the polyacrylic acid (PAA) based hydrogel using 3 wt% hydrogen peroxide (H_2O_2) is a free-radical-induced chain scission mechanism. H_2O_2 generates hydroxyl radicals (·OH), which attack the carbon–carbon backbone of PAA, cleaving it into low-molecular-weight oligomers. The crosslinked network formed by N,N'-methylenebisacrylamide (MBAA) is also disrupted through oxidative cleavage, resulting in the breakdown of the hydrogel matrix into water-soluble products. The main degradation products are low-molecular-weight PAA oligomers with terminal carboxyl and hydroxyl groups. This is supported by gel permeation chromatography (GPC) analysis (Supplementary Table 1), where the number-average molecular weight decreased from ~19000 g/mol in the pristine hydrogel to ~1407 g/mol after degradation.

Supplementary Table 1. Molecular weight analysis of pristine and degraded hydrogels measured by GPC.

Sample name	Retention time (min)	Mn (g/mol)	Mw (g/mol)	Mp (g/mol)	Polydispersity
Pristine-1	14.940	19867	24975	20716	1.257108
Pristine-2	14.983	19400	23550	19922	1.213951
Degraded	17.630	1407	1418	1342	1.008286

Mn: number-average molecular weight. Mw: weight-average molecular weight. Mp: peak molecular weight.

Supplementary Note 2: Recycling mechanisms and performance of the ReCLEAR hydrogel.

ReCLEAR hydrogel can be recycled by adding additional acrylic acid (AA) monomers, water, crosslinker, and initiator, followed by heating to trigger free-radical polymerization. Although the majority of the original carbon double bonds (C=C) are destroyed during degradation, the newly introduced AA monomers provide reactive sites for network reconstruction. Residual oligomers act as fillers, while the regenerated polymer network retains similar chemical functionality to the original. As all degradation products remain in the recycled hydrogel, its composition slightly differs from that of the pristine one. However, key functional groups (e.g., carboxyl groups) and the polymer backbone are preserved, resulting in comparable chemical properties of pristine and recycled hydrogels, supported by Fourier-transform infrared (FTIR) analysis (Supplementary Fig. 1).

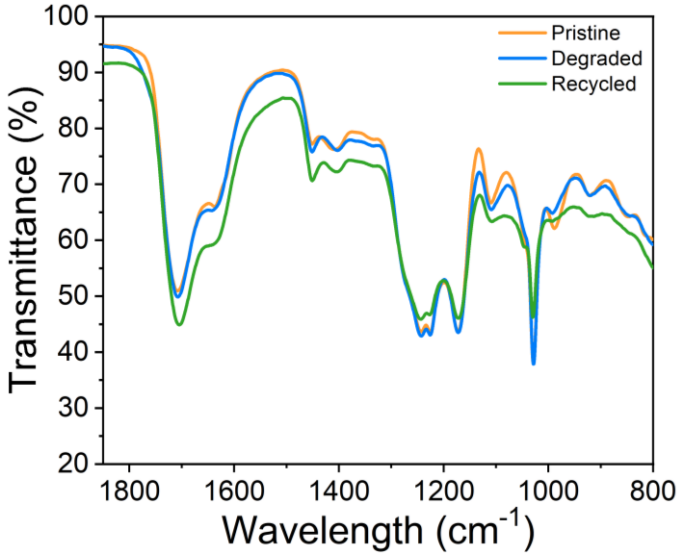

Supplementary Fig. 1 | FTIR spectra between pristine, degraded, and recycled ReCLEAR hydrogel. The ReCLEAR hydrogel maintains its chemical structure after degradation and recycling.

All samples show characteristic C=O stretching (~1700 cm^{-1}) and sulfonate (1050–1250 cm^{-1}, ~1030 cm^{-1}) peaks from carboxyl and triflate groups (COO^- and SO_3^-), respectively. The degraded sample shows a small increase in C=C stretching (~1630

cm^{-1}), indicating partial depolymerization and vinyl group regeneration. In the recycled hydrogel, the C=C signal remains, suggesting incomplete re-polymerization. Zinc cations (Zn^{2+}) coordination contributes to shifts and broadening in COO^{-}/C=O regions, while triflate signatures overlap with the C–O signal of PAA. These spectral changes validate the chemical transitions during degradation and recycling.

The pristine hydrogel weighs approximately 10 g. A minimum of 1 g AA added to the degraded solution can regenerate a hydrogel film, though with low mechanical strength. When more than 1.5 g AA is added, the recycled hydrogel forms a free-standing film with sufficient mechanical integrity for human-machine-interface applications. In this study, 2 g AA was added in each recycling cycle to achieve mechanical strength comparable to the pristine hydrogel. We have successfully tested five recycling cycles. All recycled hydrogels exhibit similar molecular weights (Supplementary Table 2), indicating good stability in the recycling process. While the ReCLEAR hydrogel shows potential for recyclability beyond five cycles, the hydrogel becomes softer and generates more bubbles after 5 cycles, which may begin to affect its subsequent performance.

Supplementary Table 2. Molecular weight analysis of the ReCLEAR hydrogel with different recycling cycles, measured by GPC.

Sample name	Retention time (min)	Mn (g/mol)	Mw (g/mol)	Mp (g/mol)	Polydispersity
1st recycled	16.781	2844	3063	3205	1.077083
2nd recycled	16.770	2730	3008	3243	1.101757
3rd recycled	16.769	2993	3177	3248	1.061174
4th recycled	16.691	2611	3005	3526	1.150859
5th recycled	16.659	2984	3267	3645	1.094858

Mn: number-average molecular weight. Mw: weight-average molecular weight. Mp: peak molecular weight.

FTIR spectra of the ReCLEAR hydrogel across five recycling cycles reveal progressive changes in functional group environments (Supplementary Fig. 2). The 1st recycled film shows higher transmittance at ~1630 cm^{-1} (residual C=C in vinyl groups) and shifted carboxylate/triflate bands (1050-1250 cm^{-1}), indicating partial recovery of the polymer network. From the 2nd to 3rd cycles, spectra stabilize, suggesting reproducible recycling with similar Zn^{2+} coordination. The 4th and 5th cycles exhibit minor spectral shifts in COO^- and SO_3^- regions, reflecting subtle structural reorganizations. Overall, the system achieves chemically stable reusability after the 2nd cycle.

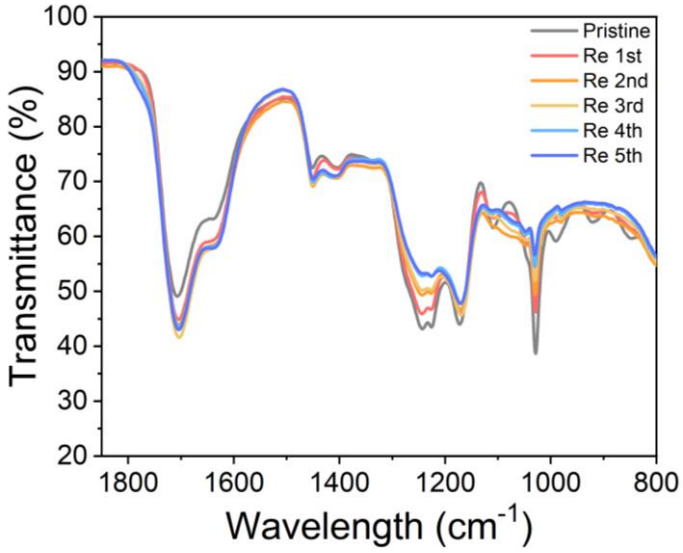

Supplementary Fig. 2 | FTIR spectra between pristine and recycled ReCLEAR hydrogels over five recycling cycles. Re: recycled.

The hydrogel maintained consistent TE performance over multiple recycling cycles (Supplementary Fig. 3). The slight increase observed in the second recycled sample is likely due to more stable coordination between Zn^{2+} ions and carboxyl groups. In contrast, the gradual decrease in TE output with additional recycling cycles is attributed to minor material loss during the transfer process.

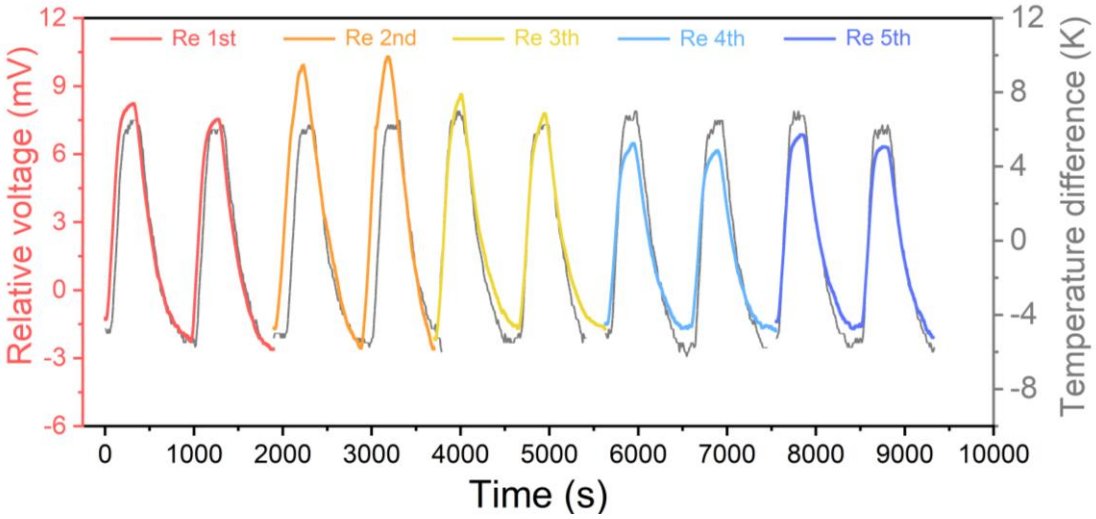

Supplementary Fig. 3 | Relative thermal voltages of recycled ReCLEAR hydrogels over five recycling cycles. Re: recycled.

Supplementary Note 3: Mechanism of thermodiffusive ionic thermoelectric materials.

Ionic thermoelectric (TE) materials function via two mechanisms for heat-to-voltage conversion. One is the thermogalvanic effect, which occurs through redox reactions of ions. The other mechanism is the Soret effect, which arises from the thermal diffusion of ions. In our ionic TE system based on PAA hydrogel containing zinc trifluoromethanesulfonate ($Zn(OTf)_2$), the TE performance is predominantly governed by thermal diffusion, as $Zn(OTf)_2$ does not undergo redox reactions within this hydrogel matrix. We use the Seebeck coefficient (S_i) to quantify the TE performance resulting from ionic migration under a temperature gradient.

The ionic flux in the thermodiffusive ionic TE system[1–3] is determined by three key factors: ionic concentration changes, voltage gradients, and temperature gradients, which can be expressed mathematically as,

$$J_i = -Di\left[\nabla n_i + \frac{q_i n_i}{k_B T}\nabla V + \frac{(\overline{\overline{s_i}} - s_i)n_i}{k_B\, T}\nabla T\right] \tag{1}$$

Where D_i is the diffusion coefficient, n_i is the ionic concentration, s_i is the partial entropy, ∇V is the voltage gradient, and ∇T is the temperature gradient.

Under steady-state conditions, the net ionic current is zero,

$$\sum_i q_i J_i = 0 \tag{2}$$

Assuming near-equilibrium conditions, the concentration profile can be described as,

$$n_i(r) = n_i^0 + \delta n_i(r) \tag{3}$$

where $\delta n_i \ll n_i^0$. Under equilibrium conditions, ∇V and ∇T across the electrodes are negligible, then,

$$\frac{q_i \nabla V}{k_B T} \ll \frac{n_i^0}{\delta n_i}, \qquad \frac{(\overline{\overline{s_i}} - s_i)n_i}{k_B\, T}\nabla T \ll \frac{n_i^0}{\delta n_i} \tag{4}$$

Then equation (3) can be derived,

$$-q_i Di\left[\nabla \delta n_i + \frac{q_i n_i^0}{k_B T}\nabla V + \frac{(\overline{\overline{s_i}} - s_i)n_i^0}{k_B\, T}\nabla T\right] = 0 \tag{5}$$

$$\sum_i \left(\frac{q_i^2 n_i^0 D_i}{k_B T} \nabla V + \frac{q_i^2 n_i^0 D_i (\overline{\overline{s_i}} - s_i)}{k_B T} \nabla T \right) = 0 \tag{6}$$

Given $\nabla \delta n_i$ is also quite small, the thermodiffusive thermopower can be expressed as,

$$S_i = -\frac{\nabla V}{\nabla T} = \frac{\Sigma q_i (\overline{\overline{s_i}} - s_i) n_i D_i}{\sum q_i^2 n_i D_i} \tag{7}$$

In the ionic TE system, where electrolytes are balanced, $q_+ = q_-$ and $n_+^0 = n_-^0$. The equation (7) can be simplified to,

$$S_i = \frac{D_+ (\overline{\overline{s_+}} - s_+) - D_- (\overline{\overline{s_-}} - s_-)}{e(D_+ + D_-)} \tag{8}$$

According to Einstein's relation in thermal mobility, the thermal mobility μ_i^T is,

$$\mu_i^T = \frac{D_i (\overline{\overline{s_i}} - s_i)}{k_B T} \tag{9}$$

The Eastman entropy of transfer relates to the ratio between thermal mobility and ionic mobility. Consequently, the ion mobility can be expressed as,

$$\mu_i^q = \frac{q_i D_i}{k_B T} \tag{10}$$

Then, the equation (8) can be further simplified as,

$$S_i = \frac{\mu_+^T - \mu_-^T}{\mu_+^q + \mu_-^q} \tag{11}$$

This relationship demonstrates that the Seebeck coefficient is fundamentally determined by the differences in thermal mobilities between cations and anions. In thermodiffusive ionic TE materials, a larger difference in thermal mobility between the ions results in enhanced thermopower generation.

Supplementary Note 4: Power factor and ZT_i value of the ReCLEAR hydrogel.

The power factor (PF_i) of ionic TE materials can be expressed as,

$$PF_i = {S_i}^2\sigma \tag{12}$$

where S_i is the ionic Seebeck coefficient and σ is the electrical conductivity. The electrical conductivity can be calculated by,

$$\sigma = \frac{L}{RA} \tag{13}$$

where L is the sample thickness between the test electrodes, R is the bulk resistance obtained from the Nyquist plot, and A is the cross-sectional area of the samples.

Based on the data presented in Supplementary Figs. 23-24 and Supplementary Table 6, our ReCLEAR hydrogel exhibits an ionic conductivity of 1.9 mS cm^{-1}, resulting in a PF_i value of 0.2 $\mu Wm^{-1}K^{-2}$.

The dimensionless figure-of-merit ZT of the TE materials, which represents the TE energy conversion efficiency, is defined as:

$$ZT = \frac{S^2\sigma}{k}T \tag{14}$$

where T is the absolute temperature and k is the thermal conductivity.

According to Supplementary Fig. 25 and Supplementary Table 7, the thermal conductivity of our ReCLEAR hydrogel is 0.48 W/m·K, yielding a ZT_i value of 1.30×10^{-4}.

Supplementary Figures

Supplementary Fig. 4 | Photograph of the ReCLEAR hydrogel. The ReCLEAR hydrogel exhibits excellent transparency, stretchability, and adhesion.

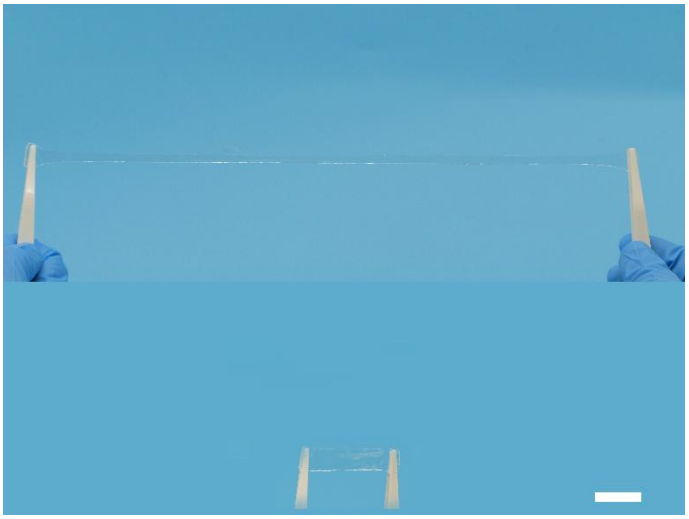

Supplementary Fig. 5 | Photographs of the stretchable pristine ReCLEAR hydrogel. The scale bar is 1 cm.

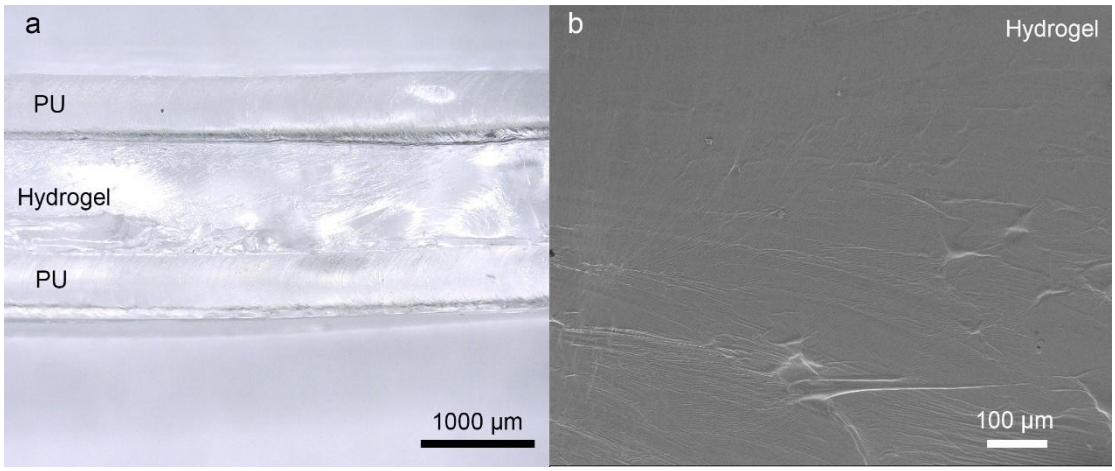

Supplementary Fig. 6 | Cross-sectional view of the ReCLEAR device and hydrogel. **a,** Optical microscope (OM) image of the ReCLEAR device cross-section. The thickness of the ReCLEAR hydrogel is approximately 1 mm, and the thickness of the PU layer is around 0.6 mm. **b,** Scanning electron microscope (SEM) image of the ReCLEAR hydrogel cross-section, showing a smooth surface with no observable microstructure.

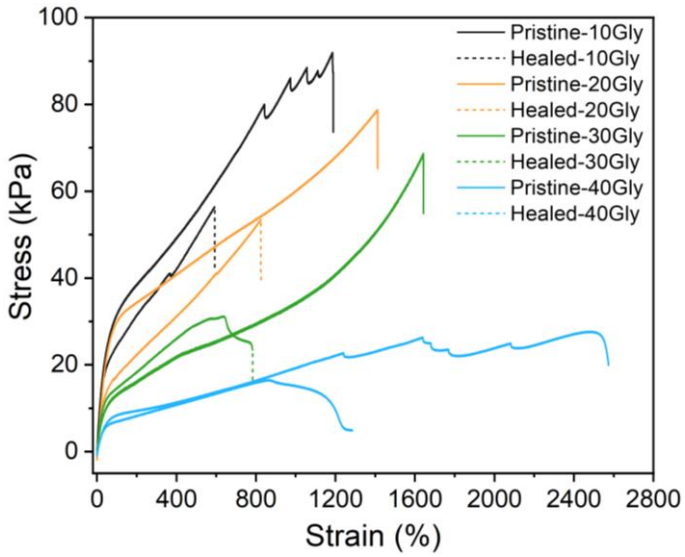

Supplementary Fig. 7 | Stretchability of pristine and self-healed hydrogels with different glycerol concentrations. All samples were healed at room temperature for 3 days. Gly: glycerol weight concentrations (wt%).

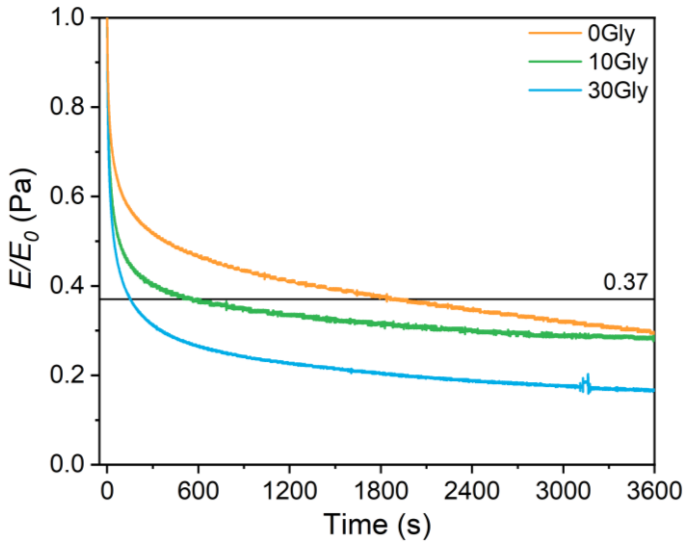

Supplementary Fig. 8 | Viscoelasticity of the hydrogel measured by dynamic mechanical analysis (DMA) with different glycerol concentrations. E/E_0 represents the loss factor of the hydrogel. Gly: glycerol weight concentrations (wt%).

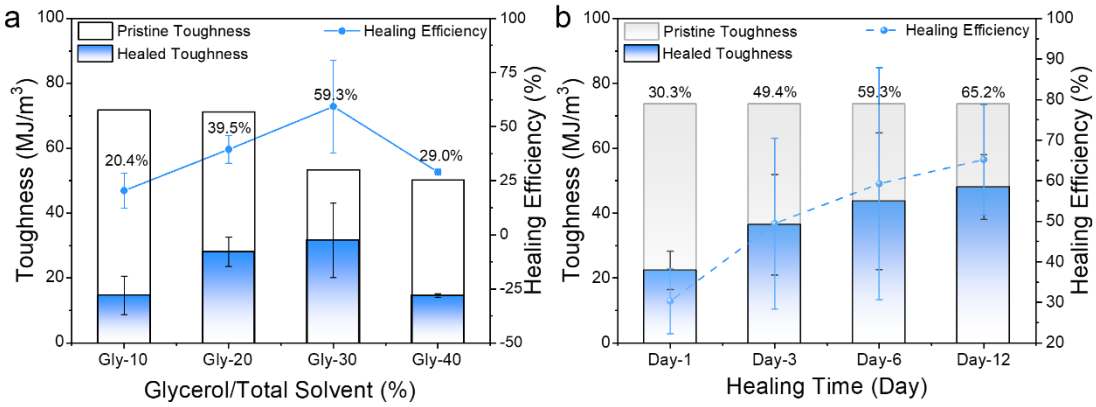

Supplementary Fig. 9 | Toughness and healing efficiencies of the hydrogel. a, Pristine and healed hydrogels with different glycerol concentrations. **b,** Hydrogel with 30 wt% glycerol after different healing durations. Gly: glycerol weight concentrations (wt%). Data are presented as mean values and the error bars represent the standard deviation, n = 5.

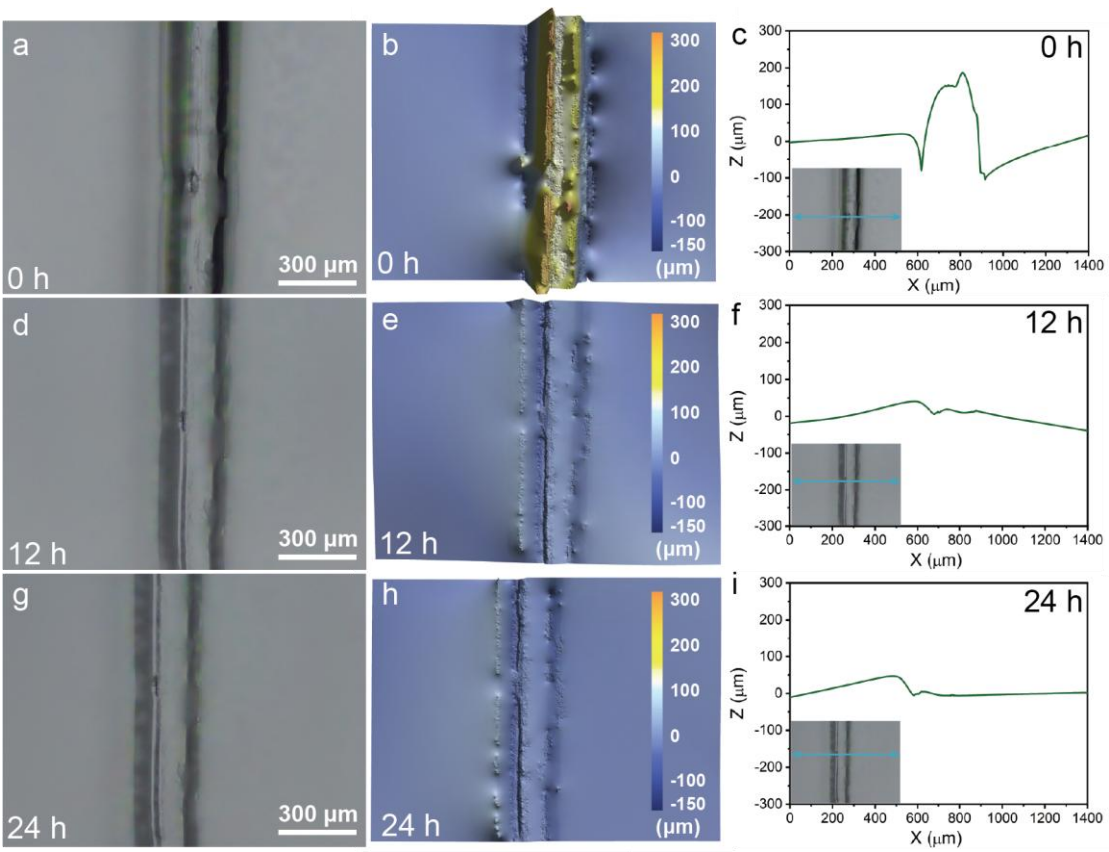

Supplementary Fig. 10 | 3D surface maps and corresponding height profiles of the ReCLEAR hydrogel at different self-healing stages within 24 h. a, d, and g, Optical images of self-healed ReCLEAR at 0 h, 12 h, and 24 h, respectively. **b, e, and h,** 3D surface profiles of self-healed ReCLEAR at 0 h, 12 h, and 24 h, respectively. **c, f, and i,** Cross-area height profiles of self-healed ReCLEAR at 0 h, 12 h, and 24 h, respectively.

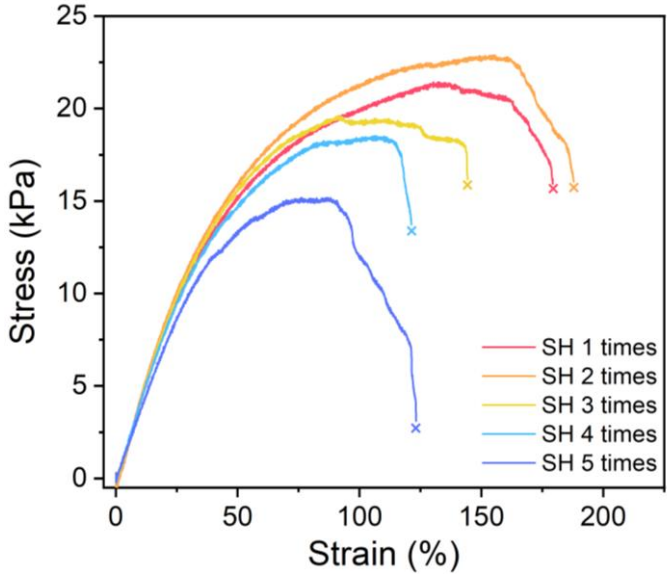

Supplementary Fig. 11 | Self-healing performance of the ReCLEAR hydrogel after 1 to 5 self-healing cycles, each with a 24 h healing period. SH: self-healed.

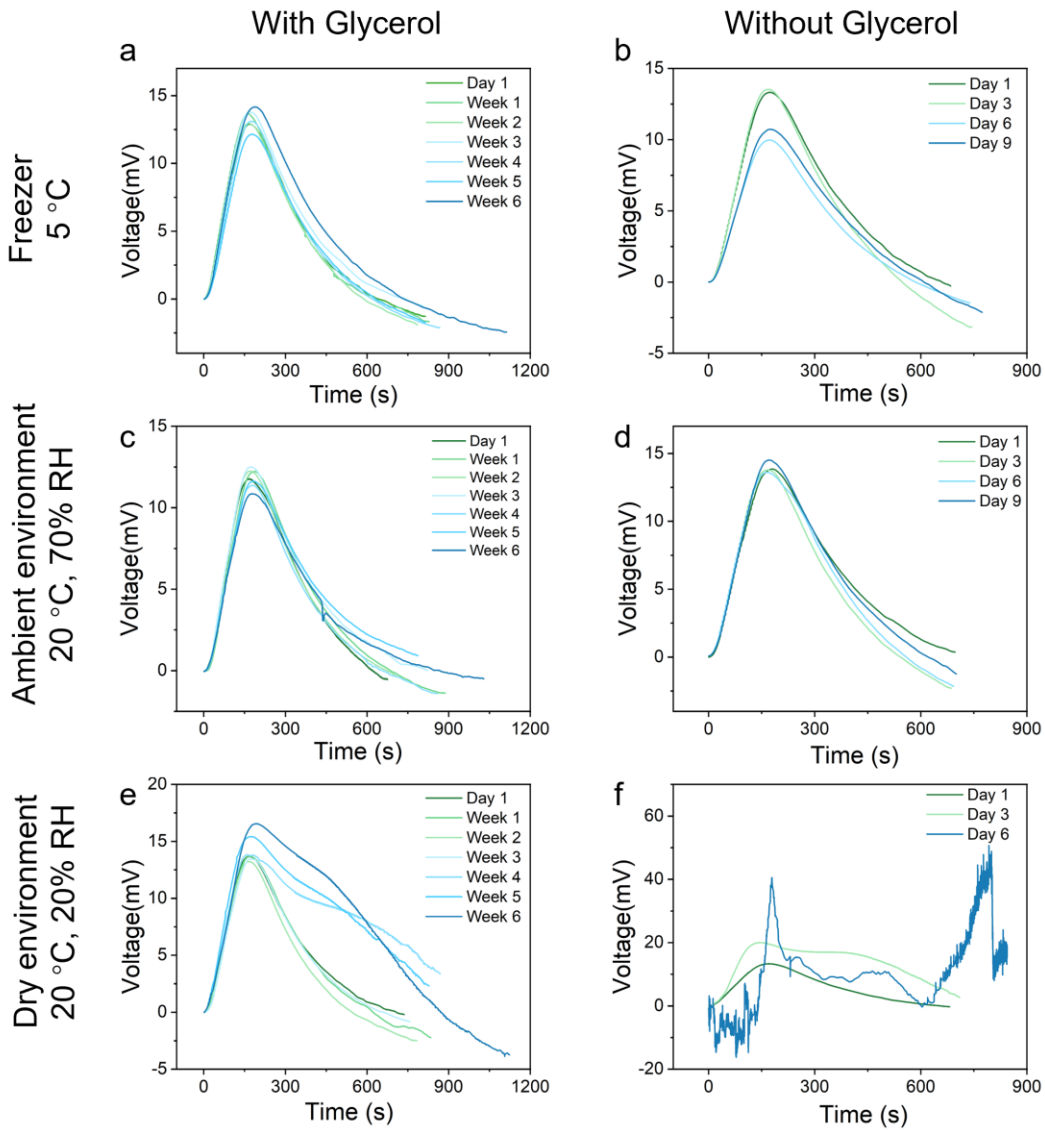

Supplementary Fig. 12 | Durability of the ReCLEAR hydrogel. a, c, and e, Thermoelectric performance of ReCLEAR hydrogel over six weeks under freezer, ambient environment, and dry environment conditions, respectively. **b, d, and f,** Thermoelectric performance of the hydrogel without glycerol over several days under the corresponding conditions.

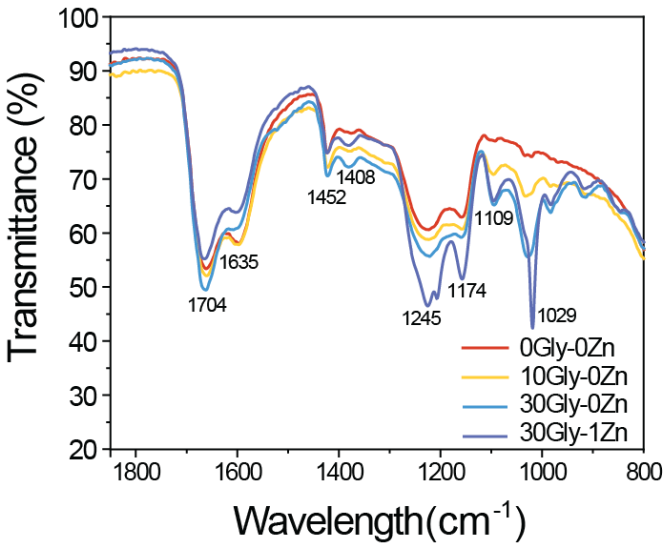

Supplementary Fig. 13 | FTIR spectra of PAA hydrogel with different glycerol contents and zinc salts. Gly: glycerol weight concentrations (wt%). Zn: $Zn(OTF)_2$ molar concentrations (M).

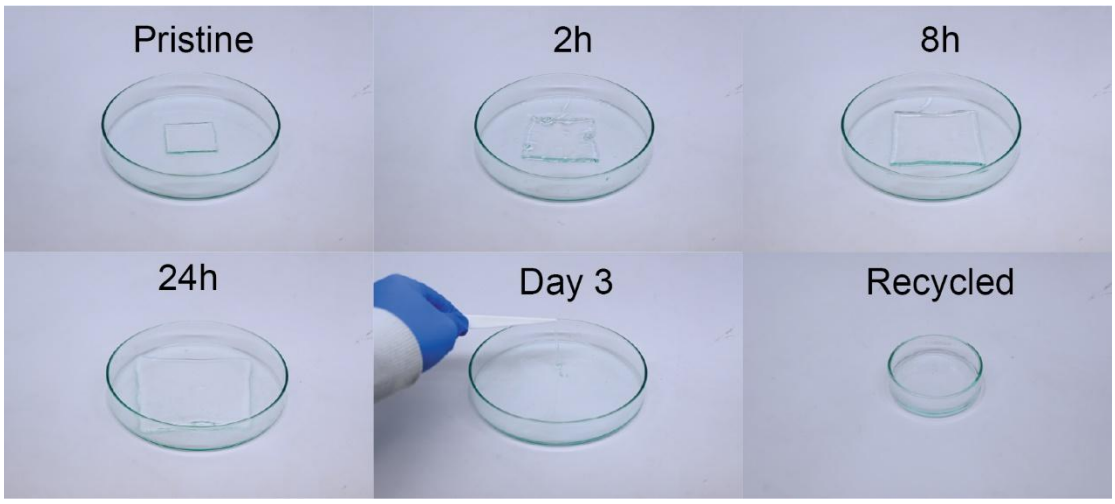

Supplementary Fig. 14 | Recycling process of a ReCLEAR hydrogel using 3 wt% hydrogen peroxide. The tested hydrogel size is 3 × 3 cm^2.

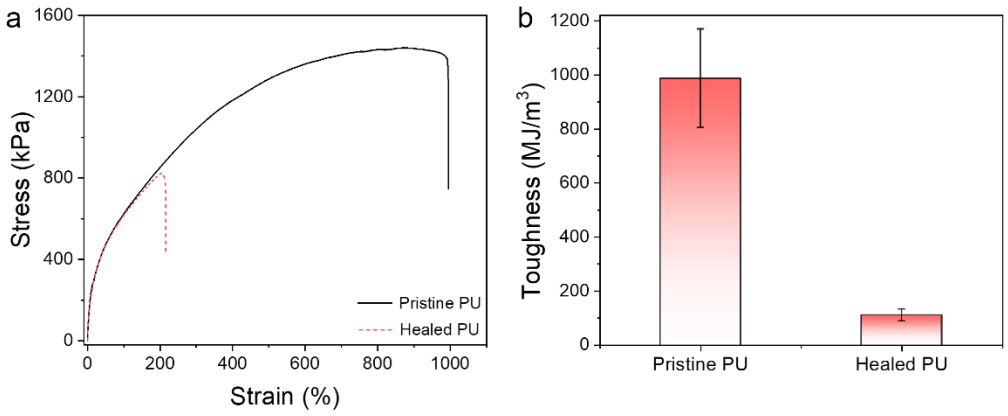

Supplementary Fig. 15 | Self-healing performance of PU layer. a, Stress-strain curves of pristine and self-healed PU layers after a healing duration of 3 days. **b,** Calculated toughness of the pristine and self-healed PU layers based on the stress-strain curves. Data are presented as mean values and the error bars represent the standard deviation, n = 5.

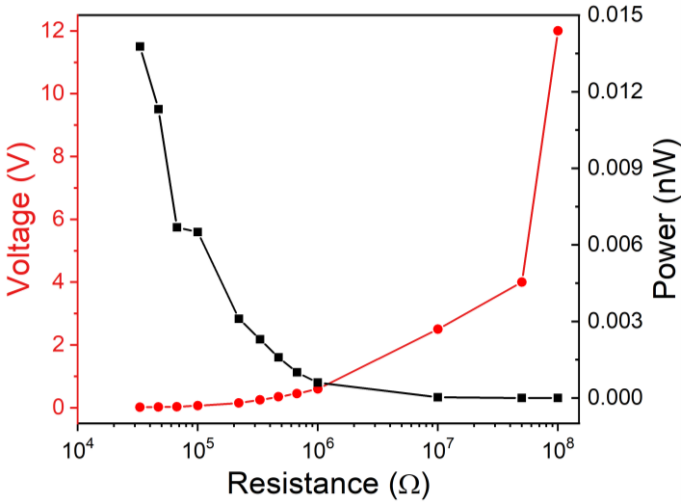

Supplementary Fig. 16 | Electrical conductivity of the PU layer. The variation of voltage and power with resistance, demonstrating the low conductivity of the PU layer.

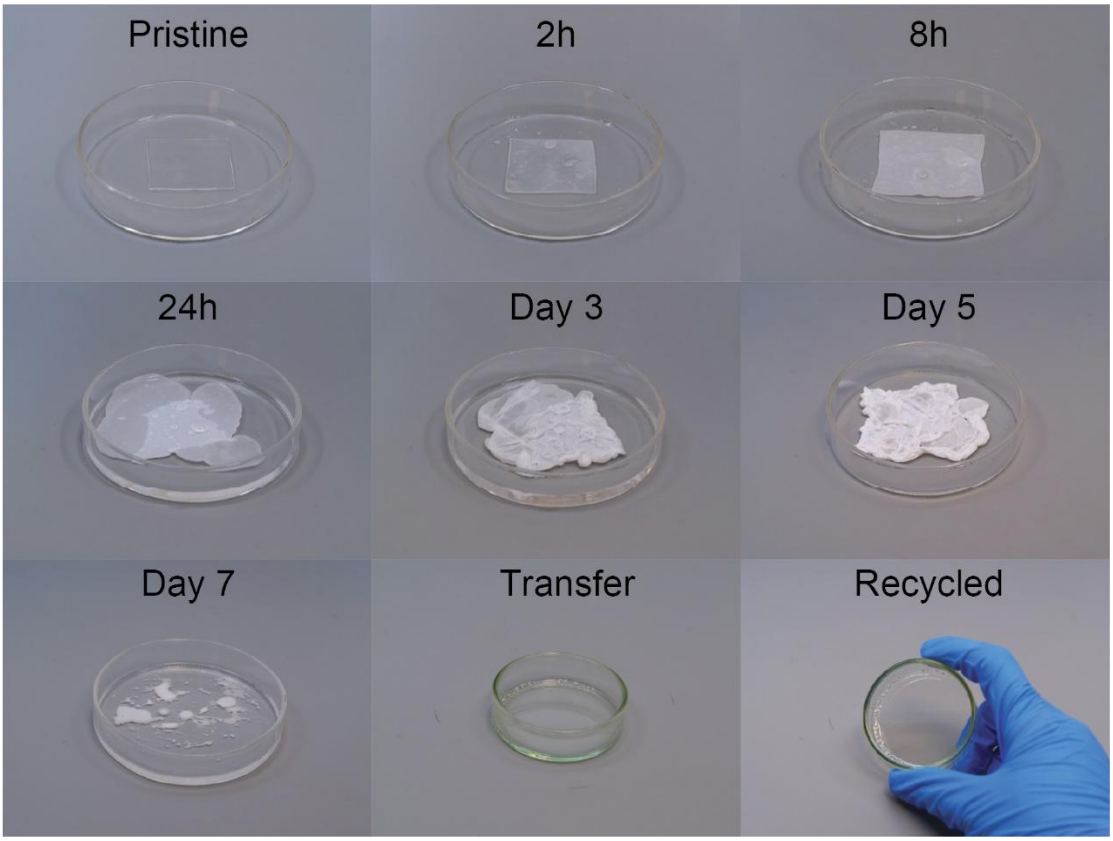

Supplementary Fig. 17 | Recycling process of a PU layer using deionized water. The tested PU size is 3 × 3 cm^2.

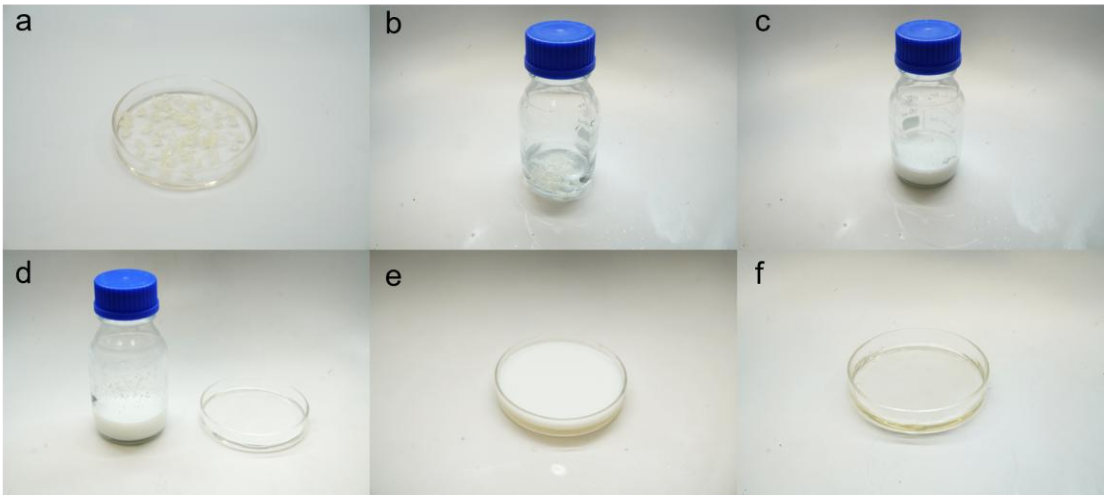

Supplementary Fig. 18 | Large-scale demonstration of the PU recycling process. a, b, Used PU layers were cut and immersed in deionized water. **c,** Water-absorbable PU dissolved in deionized water. **d-f,** The dissolved PU solution was cast into desired containers to form recycled PU layers.

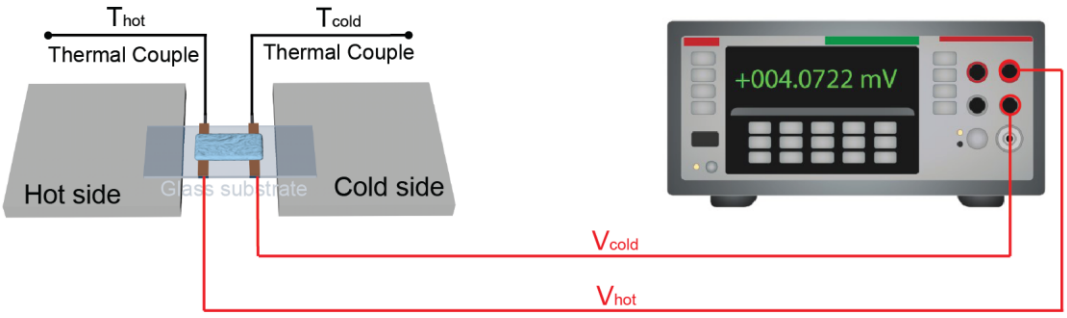

Supplementary Fig. 19 | Custom-built setup for the Seebeck coefficient measurement. A Peltier station (Ferrotec, FTA951) was used to precisely control the temperature gradient, while a Keithley multimeter (DMM6500) recorded the corresponding thermovoltage signals.

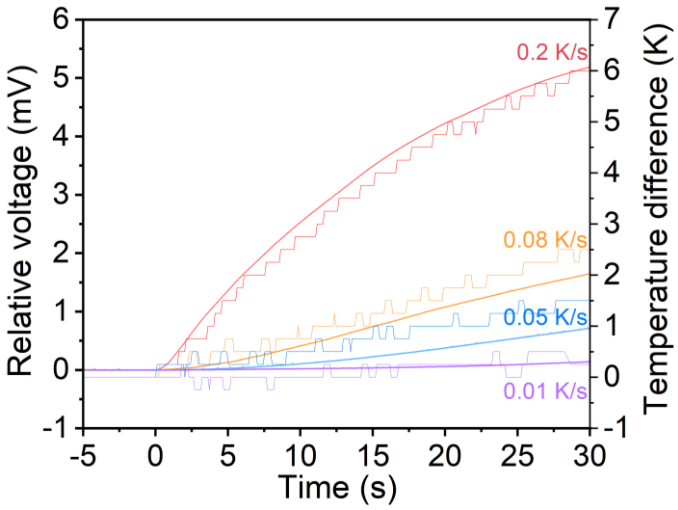

Supplementary Fig. 20 | Rapid thermoelectric responses of the ReCLEAR hydrogel under different heating rates. Step-like curves represent the temperature signal, recorded with a temperature resolution of 0.25 K.

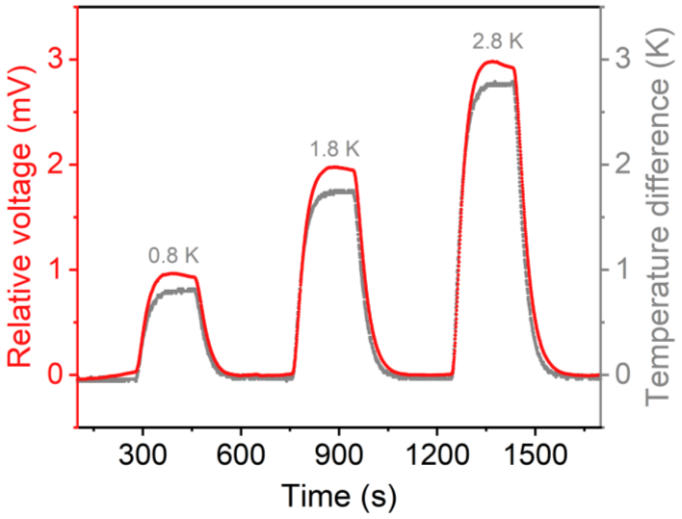

Supplementary Fig. 21 | Sensitive thermoelectric responses of the ReCLEAR hydrogel. The ReCLEAR hydrogel exhibits clear and stable thermoelectric voltage responses to small temperature fluctuations of 0.8 K, 1.8 K, and 2.8 K.

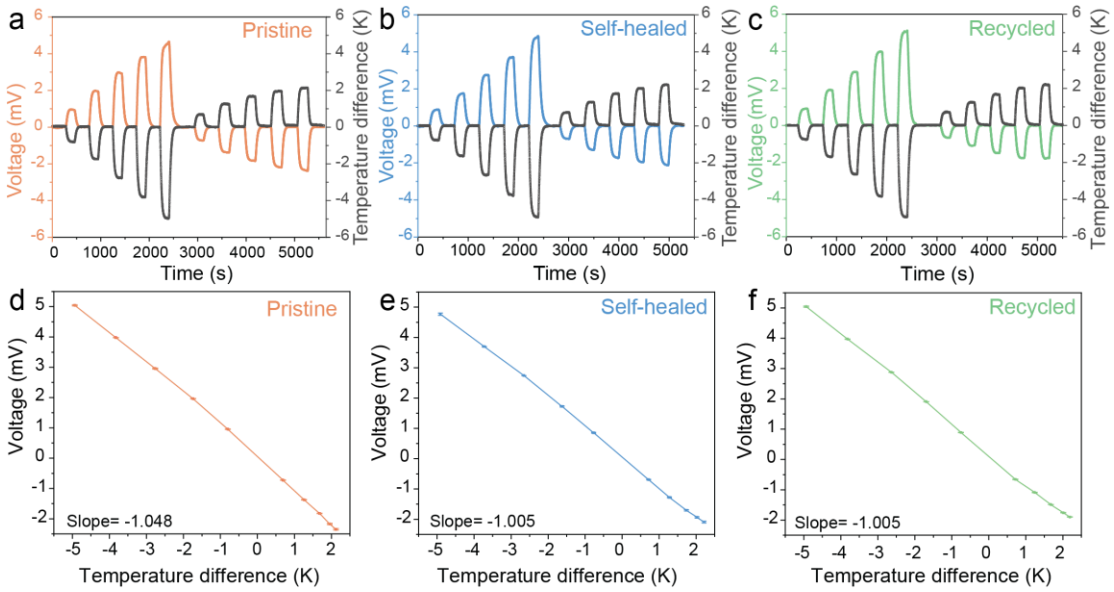

Supplementary Fig. 22 | Thermoelectric performance of pristine, self-healed, and recycled ReCLEAR hydrogels. a-c, Real-time thermal voltage outputs of pristine, self-healed, and recycled ReCLEAR hydrogels in response to different temperature changes, respectively. **d-f,** Measured thermal voltages corresponding to temperature changes, along with calculated Seebeck coefficients: pristine hydrogel (S_i = -1.048 ± 0.008 mV K^{-1}), self-healed hydrogel (S_i = -1.005 ± 0.009 mV K^{-1}), and recycled hydrogel (S_i = -1.005 ± 0.009 mV K^{-1}). Data are presented as mean values and the error bars represent the standard deviation, n = 3.

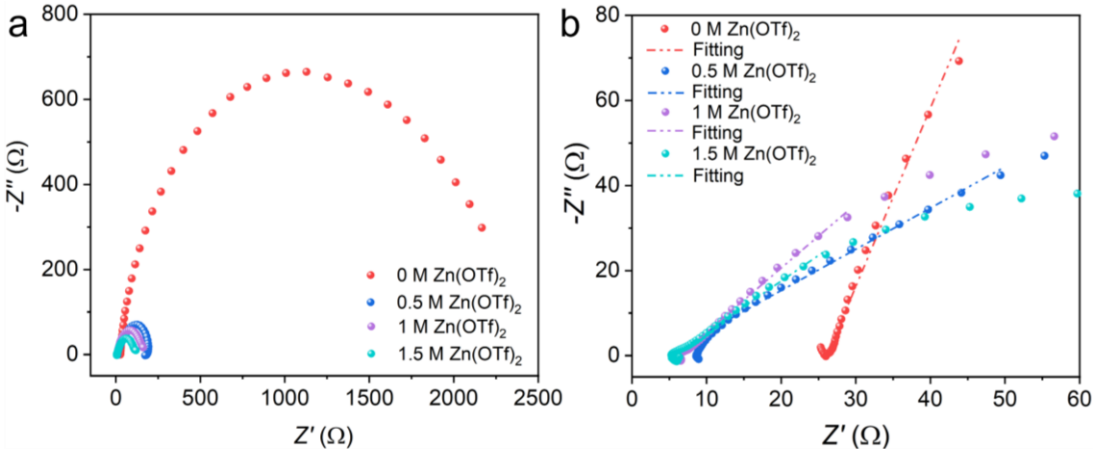

Supplementary Fig. 23 | Nyquist plots of PAA-30Gly hydrogels with different $Zn(OTf)_2$ concentrations. a, Responses from frequency 1 Hz to 100 kHz. **b,** Enlarged plots and corresponding linear fittings of Nyquist plots.

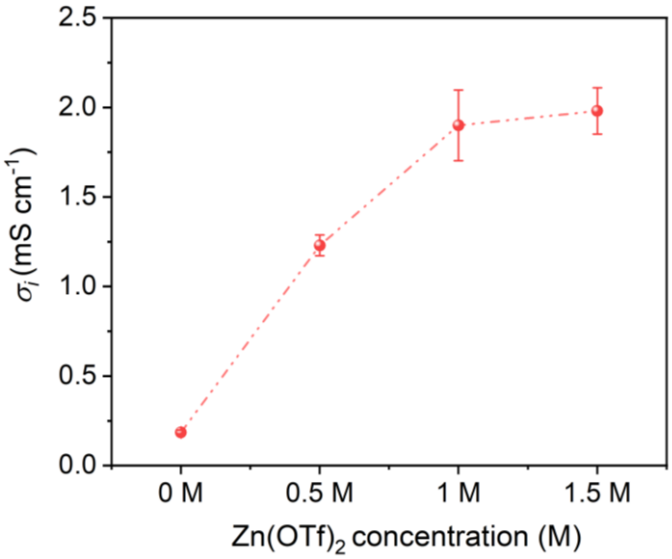

Supplementary Fig. 24 | Ionic conductivity of PAA-30Gly hydrogels with different $Zn(OTf)_2$ concentrations. Data are presented as mean values and the error bars represent the standard deviation, n = 3.

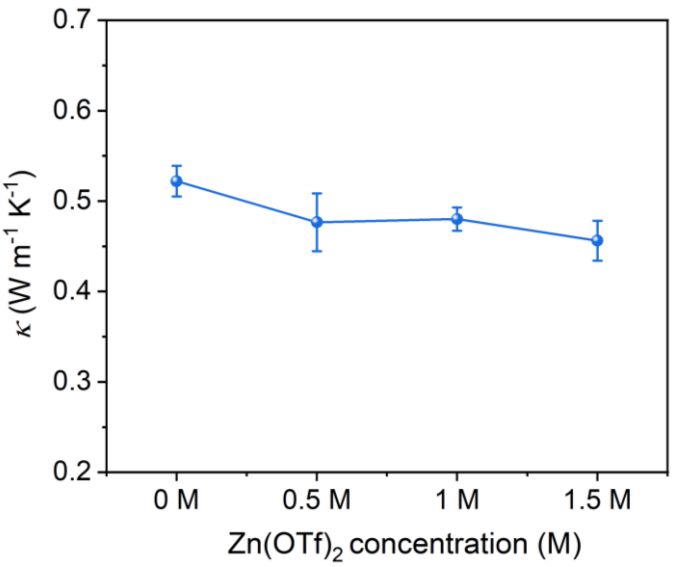

Supplementary Fig. 25 | Thermal conductivity of PAA-30Gly hydrogels with different $Zn(OTf)_2$ concentrations. Data are presented as mean values and the error bars represent the standard deviation, n = 3.

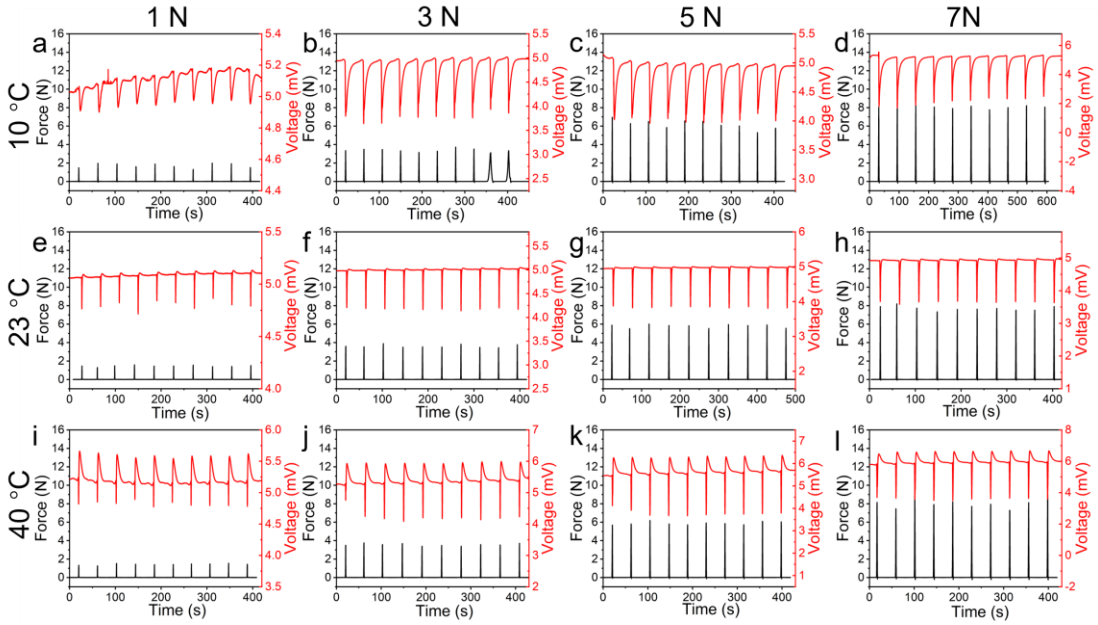

Supplementary Fig. 26 | Triboelectric performance of ReCLEAR devices under varying loading forces and temperatures. a-d, Real-time voltage outputs at 10 ℃ under loading forces of 1 N, 3 N, 5 N, and 7 N, respectively. **e-h,** Real-time voltage outputs at 23 ℃ under loading forces of 1 N, 3 N, 5 N, and 7 N, respectively. **i-l,** Real-time voltage outputs at 40 ℃ under loading forces of 1 N, 3 N, 5 N, and 7 N, respectively. Rows compare device responses under identical loading forces across different temperatures.

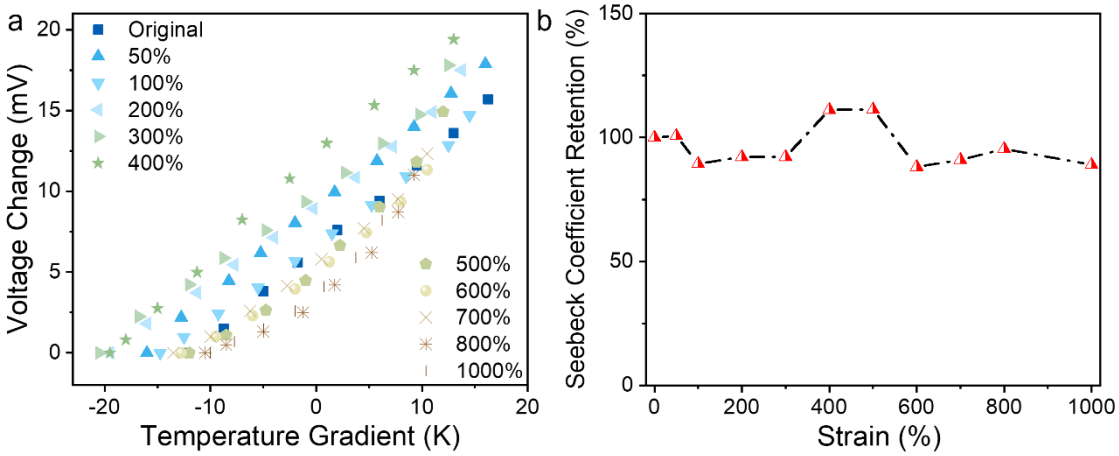

Supplementary Fig. 27 | Thermoelectric performance under different strains. a, Thermoelectric voltages under different strains. **b,** Comparison of Seebeck coefficients under different strains.

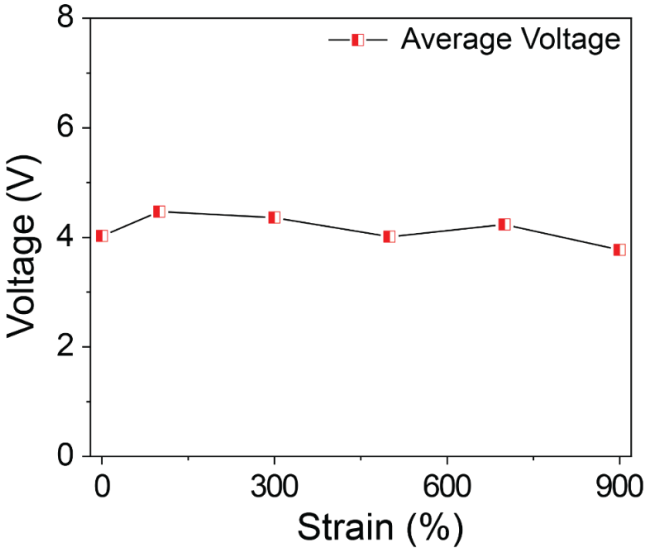

Supplementary Fig. 28 | Triboelectric performance under different strains. Average triboelectric outputs corresponding to different strains.

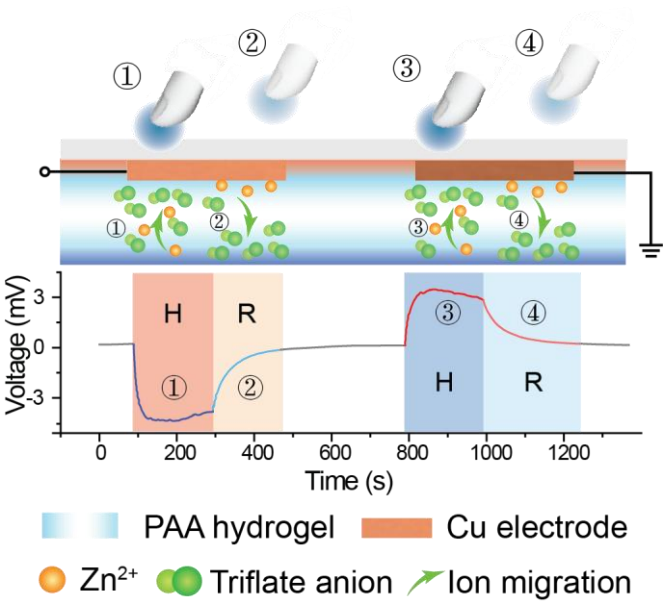

Supplementary Fig. 29 | Mechanisms of long-press signals with cold sources, dominated by the thermoelectric effect. Opposite thermoelectric signals are generated compared to hot inputs.

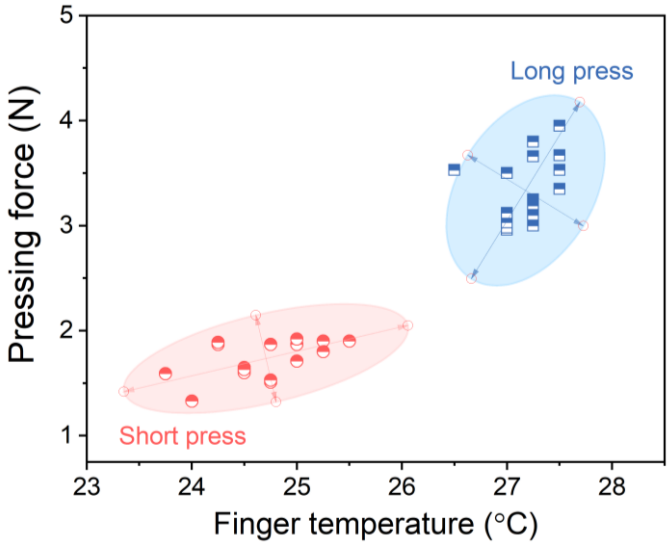

Supplementary Fig. 30 | Input distributions of finger temperature and pressing force during short and long presses by hand. The elliptical confidence region represents the 95% 2D confidence ellipse.

Supplementary Tables

Supplementary Table 3. A detailed comparison between this work and current representative thermoelectric materials for Fig. 1c in the main text.

Materials	Recyclability	Trans-parency	Eco-friendliness	Self-healing	Stretch-ability	*S* (mV/K)	Ref.
PAA/Zn(OTf)$_2$	**Full**	**Full**	**Excellent**	**Yes**	**1500%**	**-1.05**	**This work**
PI/ Bi-Te-Se/ Bi-Sb-Te/	Only PI	No	Toxic	Only PI	120%	-0.145, 0.169	39
BAA/ $Bi_{0.5}Sb_{1.5}Te_3$/ $Bi_2Te_{2.7}Se_{0.3}$	Only BAA	No	Toxic	Only BAA	N.A.	~0.23	40
PI/Bi_2Te_3/Sb_2Te_3	Only PI	No	Toxic	Only PI	50%	-0.186, 0.194	41
PEDOT: PAAMPSA:PA	No	No	Hazardous	Yes	1050%	21.9	22
PVDF-HFP/ BMIM:BF_4/ AgOTf	No	Full	Hazardous	No	N.A.	-26.4	28
Gelatin-KCl-$Fe(CN)_6^{4-/3-}$	No	No	Hazardous	No	200%	17	25
PVDF-HFP/NaTFSI/PC	No	Partially	Hazardous	No	N.A.	20	53

Supplementary Table 4. Compositions of PAA hydrogels with different glycerol grafting ratios.

Materials	Acrylic acid (g)	Water (g)	Glycerol (g)	MBAA (mg)	APS (mg)
0Gly-0Zn	4	6	0	2	30
10Gly-0Zn	4	5.4	0.6	2	30
20Gly-0Zn	4	4.8	1.2	2	30
30Gly-0Zn	**4**	**4.2**	**1.8**	**2**	**30**
40Gly-0Zn	4	3.6	2.4	2	30

APS: ammonium persulfate. Gly: glycerol weight concentrations (wt%). Zn: $Zn(OTF)_2$ molar concentrations (M).

Supplementary Table 5. Determination of $Zn(OTf)_2$ contents in different concentrations of ionic thermoelectric hydrogels.

Molar concentrations of $Zn(OTf)_2$ in recipe	Weights of $Zn(OTf)_2$ (g)
0 M	0
0.5 M	0.7634
1 M	**1.5267**
1.5 M	2.2901

Supplementary Table 6. Average values of ionic conductivity of PAA-30Gly hydrogels with different $Zn(OTf)_2$ concentrations.

Materials	Ionic conductivity ($mS\ cm^{-1}$)
PAA-30Gly-0Zn	0.1855
PAA-30Gly-0.5Zn	1.2296
PAA-30Gly-1Zn	1.9004
PAA-30Gly-1.5Zn	1.9803

Gly: glycerol weight concentrations (wt%). Zn: $Zn(OTF)_2$ molar concentrations (M).

Supplementary Table 7. Average thermal conductivity values of PAA-30Gly hydrogels with different $Zn(OTf)_2$ concentrations at different temperatures.

Materials	Temperature (K)	Thermal conductivity (W/m·K)
PAA-30Gly-0Zn	297.27	0.52204
PAA-30Gly-0.5Zn	297.21	0.47656
PAA-30Gly-1Zn	296.89	0.48016
PAA-30Gly-1.5Zn	297.41	0.45627

Gly: glycerol weight concentrations (wt%). Zn: $Zn(OTF)_2$ molar concentrations (M).

Supplementary References

1. Han, C.-G., Qian, X., Li, Q., Deng, B., Zhu, Y., Han, Z., Zhang, W., Wang, W., Feng, S.-P., Chen, G. & Liu, W. Giant thermopower of ionic gelatin near room temperature. *Science* **368,** 1091–1098 (2020).
2. Cheng, H., Le, Q., Liu, Z., Qian, Q., Zhao, Y. & Ouyang, J. Ionic thermoelectrics: principles, materials and applications. *J. Mater. Chem. C* **10,** 433–450 (2022).
3. Jia, S., Qian, W., Yu, P., Li, K., Li, M., Lan, J., Lin, Y.-H. & Yang, X. Ionic thermoelectric materials: Innovations and challenges. *Mater. Today Phys.* **42,** 101375 (2024).